Vertically coupled InP/InGaAsP microring lasers using a single epitaxial growth and single-side lithography

Óscar García López, Dries Van Thourhout, Steven Verstuyft, Manuel López-Amo, Roel Baets, and Marko Galarza

Abstract— The experimental demonstration of vertical microring lasers requiring only one single epitaxial growth and two single-side lithographic steps is presented, in what is the simplest fabrication scheme for such devices published to date. The fabricated lasers show series resistance of around 20 Ω at forward bias, threshold currents at room temperature between 35 and 58 mA, and single-mode emission with a side-lobe suppression ratio higher than 30 dB. The measured optic output power level is of tens of microwatts. The approach allows the improvement of the optical features maintaining the simplicity of the manufacturing procedure.

Index Terms—Integrated optics, semiconductor waveguides, semiconductor lasers, ring lasers.

I. INTRODUCTION

OPERATING similar to Fabry–Pérot resonators, but without the need of quality edge mirrors, microring resonators provide a sharp wavelength selectivity and a large field enhancement in a compact arrangement. Over the last years, they have been a fundamental element in a wide variety of high-performance photonic integrated devices providing optical functionalities as diverse as filtering [1], lasing [2], sensing [3], modulation [4], routing [5], switching [6], frequency comb generation [7], logic gates [8] and memories [9].

The basic layout of a ring resonator comprises a circular waveguide and one or two lateral waveguides operating as evanescent wave input and output couplers to the ring. Although being a simple structure, the high quality factors

required by the microrings imply very demanding fabrication challenges regarding the propagation loss in the ring and the coupling coefficient between the resonator and the bus waveguides. In the lateral coupling approach, the gap has to be submicron, usually requiring electron beam lithography. Moreover, since the microring and bus waveguides lay in the same epitaxial plane, the realization of functionalities that require active-passive integration is very complex. On the other hand, the vertical coupling approach containing two vertically stacked waveguide core layers, one to define the bus waveguides and the other for the microring, does allow for the definition of active-passive structures. Since the coupling between the bus and the ring waveguides, mainly depends on the thickness of the intermediate layer, which is accurately determined by the epitaxial growth, it can be controlled more precisely than on laterally coupled microring resonators. Nevertheless, wafer bonding or regrowth is usually required in order to manufacture such devices, increasing the complexity of their fabrication [10]. Furthermore, since two lithography steps are required either on each side of the wafer or after each growth step, alignment becomes a critical issue [11]. Either way, in both cases microring resonators have a definitive impact on the fabrication process of the devices of which they are part. Because of these technological specificities, the most developed approaches for InP monolithic integration do not include microring resonators as one of their basic building blocks. Butt-joint integration [12] allows the fabrication of ring lasers with larger cavities, but requires an inefficient all active approach for the coupling junction in the case of microrings [13]. The asymmetric twin-guide (ATG) technology [14, 15] neither reaches the compactness of microrings, as they have to include the gain section and two vertical tapers in the resonator [16]. The same issues apply to membrane-based schemes [17] since they also make use of a vertical integration arrangement where active and passive layers couple strongly [18].

We proposed in [19] a versatile active-passive integration approach, structurally similar to the ATG platform, but grounded on two symmetric vertical layers instead. The concept is technologically compatible with the component library of the ATG platform, since it is also based on vertical transitions between active and passive waveguides, although being in this case compatible with the design of microring
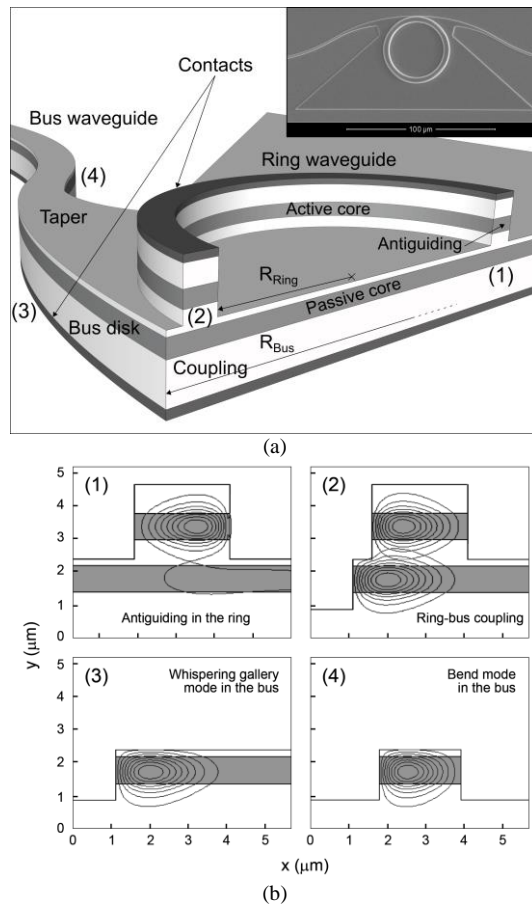
(a)

(b)

Fig. 1. a) 3D schematic picture of the fabricated microring laser. In the inset, a photograph of the fabricated device before the metallization step. b) Field distribution of the propagating modes in the ring, coupling region, bus disk, and bus waveguide.

TABLE I
DESCRIPTION, COMPOSITION, THICKNESS AND DOPING LEVEL OF THE EPITAXIAL LAYER STACK

| Description	Composition	Bandgap (µm)	Thickness (nm)	Doping
Contact layer	$In_{0.53}Ga_{0.47}As$	1.65	160	p++
p-contact	InP	0.92	1000	p++
p-contact	InP	0.92	75	p+
SCH	$In_{0.83}Ga_{0.17}As_{0.37}P_{0.63}$	1.13	190	nid
Barrier (×5)	$In_{0.83}Ga_{0.17}As_{0.37}P_{0.63}$	1.13	15	nid
QW (×6)	$In_{0.78}Ga_{0.22}As_{0.79}P_{0.21}$	1.55	8	nid
SCH	$In_{0.83}Ga_{0.17}As_{0.37}P_{0.63}$	1.13	190	nid
Interlayer	InP	0.92	580	n+
Etch-stop	$In_{0.9765}Ga_{0.0235}As_{0.05}P_{0.95}$	0.94	20	n+
Interlayer	InP	0.92	200	n+
Bus core	$In_{0.83}Ga_{0.17}As_{0.37}P_{0.63}$	1.13	800	n+
n-contact	InP	0.92	2000	n+
Substrate	InP	0.92	–	n
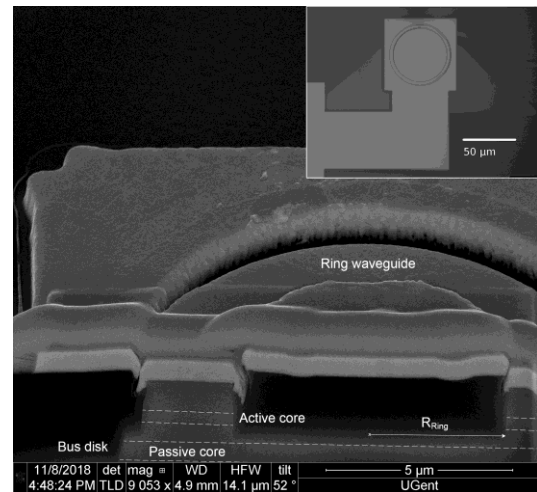
Fig. 2. SEM image of the cross section of a microring laser. The inset shows a top view photograph of the device after metallization.

resonators as well. The theoretical proposal for the development of microring resonators using this structure was published in [20]. In the current work, the proof of concept of regrowth- and wafer-bonding-free vertically coupled microring lasers is presented, which increases the set of components offered by the earlier mentioned platforms.

II. DEVICE STRUCTURE AND FABRICATION

Fig. 1(a) shows the 3D representation of the fabricated laser structure together with a top view photograph of the device prior to metallization. The key elements in the design of the laser are the two vertically coupled cores close to phase matching condition. The lower layer is passive and defines the bus waveguide, whereas the upper core is active and provides the guiding and the gain in the ring. Fig. 1(b) shows the field distribution of the propagation modes in each relevant section of the device. Light generated in the ring (1) excites the mode with the higher confinement in the active core, which is not the main even mode of the structure but the odd quasi-guided supermode. The bend loss of this strongly asymmetric mode shows an oscillatory pattern with minima below 0.1 dB/90° for radii larger than 100 µm, evolving under 1 dB/90° for smaller radii. The mode in rings beyond 30 µm seems to vanish into a radiation mode. In the coupling region (2), the

upper ring mode couples evanescently to the lower bus whispering gallery mode. The disk structure for the bus waveguide (3) avoids the need for the inner sidewall of the waveguide, simplifying drastically the placement of the ring over it. Finally, the bent bus waveguide is laterally tapered in order to guide the light into a single-mode rib structure (4). The entire design process is described in detail in [20].

The epitaxial layer structure is detailed in Table I. It essentially consists of a 0.8-µm-thick InGaAsP layer (with a bandgap cutoff wavelength of λ_g=1.13 µm), a 0.8-µm-thick InP separation layer, and a multiquantum-well (MQW) active core. The MQW region is composed of six 80-Å-thick 1% compressively strained InGaAsP (λ_g=1.55 µm) quantum wells separated by 150-Å-thick InGaAsP (λ_g=1.13 µm) barriers and sandwiched between two 190-nm-thick InGaAsP (λ_g=1.13 µm) separate confinement heterostructure (SCH) layers.

The epitaxial layers were grown by metal–organic chemical vapor deposition (MOCVD). The SiO$_x$ pattern of the rings was defined by plasma etching with conventional photoresist. The circular waveguides were etched by RIE through the active core down to the InP interlayer. Next, a selective wet etch down to the etch-stop layer using H$_3$PO$_4$:HCl (7:3) was performed to better control the depth and to reduce the lateral
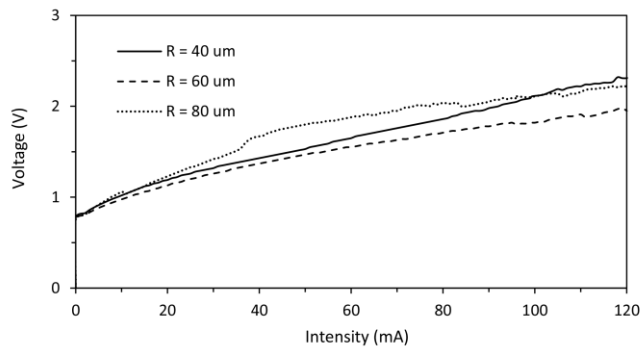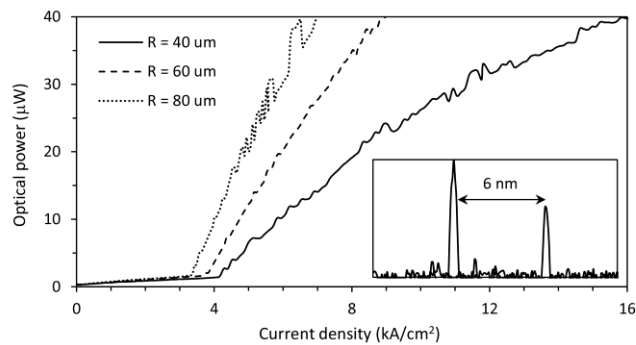
Fig. 3. V−I response of three microring diode lasers.

Fig. 4. Typical L−I characteristics of microring lasers operated in CW operation at room temperature and for three different ring radii.

Fig. 5. The output spectra of the microring lasers for three different ring radii.

roughness of the ring ridge. Subsequently, the bus waveguide was dry etched using the above-mentioned chemistry and parameters. Thereafter, polyimide was spin-coated on the sample to form an insulation layer, and removed on the ridges by plasma etch. Next, using a negative photoresist and a metal liftoff process, the metallization pattern was defined. Finally, the substrate was thinned and a back contact was deposited.

A set of microring lasers with ring radii ranging from 5 to 80 μm and a fixed bus disk radius of 100 μm were fabricated. The lateral shift between the ring and the underlying bus disk waveguide was designed at 0.5 μm for every device as a minimum defined by technology. The expected coupling factor is 4% for the smallest ring and 12% for the largest. Higher lateral misalignments imply an exponential decrease in the coupling coefficient, being reduced by half for a step of 1 μm (see [20] for a more detailed quantitative analysis). SEM pictures of the cross section of the device (Fig. 2) reveal that such submicron feature was fabricated reproducibly and measured 0.54 μm, implying a decrease of the coupling factor lower than 1% in the worst case. Pictures also confirm that the metal contact over the upper ring ridge was good.

III. DEVICE RESULTS

The devices were operated in CW operation at room temperature. Fig. 3 displays some typical electrical characteristics of the microring diodes. The devices show a low series resistance of around 20 Ω at forward bias proving a good electrical performance. Fig. 4 shows the light intensity ve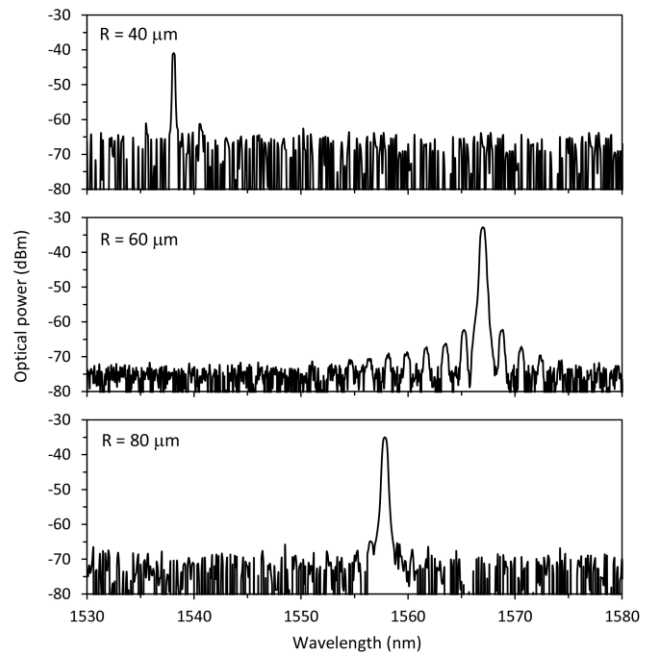rsus current density curves (L−I) of the lasers, measured in one bus waveguide. The threshold current density decreases from 4.2 to 3.3 kA/cm^2 for radii varying from 40 to 80 μm, as expected for higher coupling coefficients. The external efficiency also improves from 0.5 to 0.7 mW/A for the same radius range. Some curves exhibit small ripples corresponding to longitudinal mode hopping in the amplifying ring section. The inset shows a shift of 6 nm in the optical spectrum for a ring of 80 μm at both sides of one of these folds. Such multimode lasing spectra could be avoided defining a lateral grating on the ring waveguide during lithography in order to favor the desired mode [21]. Lasing was observed for temperatures up to 60 °C.

Nevertheless, in absolute terms, the lasers emitted less optical power than expected. Using pulsed current injection (2 μs pulse width and 2 % duty cycle), the power increases to several tenths of milliwatts due to a better thermal performance in this regime, but these values are still lower than predicted. Furthermore, devices with the ring radius smaller than 40 μm did not exhibit lasing. In addition to sidewall roughness in such highly confined structures, surface recombination of injected carriers is one of the major limiting factors to good laser performance. Therefore, optimizing the dry etch process and coating the etched surface with a layer of SiO$_2$ or passivating it with Al$_2$O$_3$ by atomic layer deposition (ALD) [22] are expected to drastically reduce these sources of loss. The use of quantum dots (QDs) instead of quantum wells as the active media has also shown to be a good strategy to minimize the recombination on the resonator surface and achieve lower threshold lasing in small volume cavities [23]. Furthermore, since the analysis of structures with microbends is always difficult, even more so with two bend waveguides of different curvatures [20], the optical losses in the ring waveguide and the coupling region might be underestimated.

Nevertheless, the technological simplicity of the structure allows overcoming the mentioned drawbacks without adding extra steps to the manufacturing procedure. Thus, in the ring section, by limiting the underlying slab passive waveguide to a broad (but finite) mesa waveguide, the asymmetry between the waveguides is preserved and the bend losses can be reduced, as proposed in [20]. On the other hand, the inefficiency of the coupler in small rings might be improved by choosing the same curvature for the underlying disk bus waveguide and the ring guide, thus increasing the coupling length and the efficiency. Future devices with smaller diameters and improved processing are expected to result in lower thresholds and higher power operation.

Fig. 5 depicts the measured output spectra of the working microring lasers, for different pump injection currents. The lasers show single-mode operation with a side-lobe suppression ratio higher than 30 dB for these operating conditions. Such performance might be due to dependency of the bending losses of the strongly asymmetric mode in the ring with the wavelength. Due to the total lateral symmetry of the structure, the lasers generate light in both opposite directions, exciting counter-propagating degenerate modes that couple to each other through scatterings or imperfections. If unidirectional lasing is required by the application, several technological strategies that are compatible with the structure of these lasers could be used, such as the definition of crossover S-bend waveguides in the ring cavity [24].

IV. CONCLUSION

In this work, a new vertical microring laser using a single epitaxial growth on InP and conventional single-side lithography has been successfully demonstrated. The approach is based on two vertically coupled cores close to phase matching condition and avoids the need of complex fabrication processes such as electron beam lithography, wafer bonding or epitaxial regrowth. The lasers with radii bigger than 40 μm show good electrical and optical characteristics. Smaller rings do not reach lasing due to surface recombination, propagation losses in the cavity and the reduced coupling factor because of the radius mismatch between the upper ring and the underlying disk waveguide. Such drawbacks can be easily overcome defining a broad rib waveguide in the bus core layer under the ring and reducing the curvature of the bus disk in the coupling region. Such improvements would not increase the complexity of the fabrication scheme.

REFERENCES

[1] L. Xu et al., "Silicon-on-insulator-based microwave photonic filter with widely adjustable bandwidth," *Photonics Res.*, vol. 7, no. 2, pp. 110–115, Feb. 2019.

[2] B. Midya et al., "Supersymmetric microring laser arrays," *Photonics Res.*, vol. 7, no. 3, pp. 363–367, Mar. 2019.

[3] H. Ren et al., "Dissipative sensing with low detection limit in a self-interference microring resonator," *J. Opt. Soc. Am. B.*, vol. 36, no. 4, pp. 942–951, Apr. 2019.

[4] S. Pal and S. Gupta, "Performance analysis of an electrostatic doping assisted silicon microring modulator," *Opt. Commun.*, vol. 430, pp. 131–138, Jan. 2019.

[5] L. Liu et al., "Compact and broadband optical add-drop de-multiplexer with cascaded elliptical micro-rings on SOI," *IEEE Photonic Tech. L.*, vol. 31, no. 6, pp. 451–454, Mar. 2019.

[6] Q. Cheng et al., "Scalable microring-based silicon Clos switch fabric with switch-and-select stages," *IEEE J. Sel. Topics Quantum Electron.*, vol. 25, no. 5, Sep./Oct. 2019, Art. no. 3600111.

[7] M. Zhang et al., "Broadband electro-optic frequency comb generation in a lithium niobate microring resonator," *Nature*, vol. 568, pp. 373–377, Mar. 2019.

[8] A. Godbole et al., "All optical scalable logic gates using Si$_3$N$_4$ microring resonators," *IEEE J. Sel. Topics Quantum Electron.*, vol. 22, no. 6, Nov./Dec. 2016, Art. no. 5900308.

[9] J. Zhang et al., "Optical dynamic memory based on an integrated active ring resonator," *Opt. Lett.*, vol. 43, no. 19, pp. 4687–4690, Oct. 2018.

[10] D. Liang et al., "Electrically-pumped compact hybrid silicon microring lasers for optical interconnects," Opt. Express, vol. 17, no. 22, pp. 20355–20364, Oct. 2009.

[11] C. W. Tee, K. A. Williams, R. V. Penty, and I. H. White, "Fabrication-tolerant active–passive integration scheme for vertically coupled microring resonators," *IEEE J. Sel. Topics Quantum Electron.*, vol. 12, no. 1, pp. 108–116, Jan./Feb. 2006.

[12] M. Smit et al., "An introduction to InP-based generic integration technology," *Semicond. Sci. Technol.*, vol. 29, no. 8, p. 083001, 2014.

[13] M. T. Hill et al., "A fast low-power optical memory based on coupled micro-ring lasers," *Nature*, vol. 432, pp. 206–209, Nov. 2004.

[14] V. M. Menon, F. Xia, and S. R. Forrest, "Photonic integration using asymmetric twin-waveguide (ATG) technology: Part II—Device," *IEEE J. Sel. Topics Quantum Electron.*, vol. 11, no. 1, pp. 30–42, Jan./Feb. 2005.

[15] V. Tolstikhin, "Regrowth-free multi-guide vertical integration in InP for optical communications," in Proc. IPRM, Berlin, Germany, May 2011.

[16] V. M. Menon, W. Tong, and S. R. Forrest, "Control of quality factor and critical coupling in microring resonators through integration of a semiconductor optical amplifier," *IEEE Photon. Technol. Lett.*, vol. 16, no. 5, pp. 1343–1345, May 2004.

[17] J. G. M. van der Tol et al., "Indium phosphide integrated photonics in membranes," *IEEE J. Sel. Topics Quantum Electron.*, vol. 24, no. 1, Jan./Feb. 2018, Art. no. 6100809.

[18] Y. Jiao et al., "First demonstration of an electrically pumped laser in the InP membrane on silicon platform," in Advanced Photonics 2015, OSA Technical Digest (online) (Optical Society of America, 2015), paper IM4B.3.

[19] O. G. López, D. Lasaosa, M. López-Amo, and M. Galarza, "Highly efficient fully resonant vertical couplers for InP active passive monolithic integration using vertically phase matched waveguides," *Opt. Express*, vol. 21, no. 19, pp. 22717–22727, Sep. 2013.

[20] O. G. López, D. Van Thourhout, D. Lasaosa, M. López-Amo, R. Baets, and M. Galarza, "Vertically coupled microring resonators using one epitaxial growth step and single-side lithography," *Opt. Express*, vol. 23, no. 4, pp. 5317–5326, Feb. 2015.

[21] A. Arbabi, S. M. Kamali, E. Arbabi, B. G. Griffin, and L. L. Goddard, "Grating integrated single mode microring laser," *Opt. Express*, vol. 23, no. 4, pp. 5335–5347, Feb. 2015.

[22] Y. Wan et al., "Low-threshold continuous-wave operation of electrically pumped 1.55 μm InAs quantum dash microring lasers," *ACS Photon.*, vol. 6, no. 2, pp. 279–285, Dec. 2018.

[23] Y. Wang et al., "Sub-wavelength InAs quantum dot microdisk lasers epitaxially grown on exact Si (001) substrates," *Appl. Phys. Lett.*, vol. 108, no. 22, 2016, Art. no. 221101.

[24] J. Ren et al., "Unidirectional light emission in PT-symmetric microring lasers," *Opt. Express*, vol. 26, no. 21, pp. 27153–27160, Oct. 2018.